A Procedural Body Decomposition System in Houdini

Forensic Grounding, Technical Implementation and Verification of a Houdini Digital Asset for Staged Human Decomposition

Research and Development Thesis Report

Author: [Abhimanyu Ravichandran]

Unit: MSc Master Project, National Centre for Computer Animation, Bournemouth University

Date: 17 August 2026

Submitted build: body_decomp_18.hipnc

Abstract

In film and video games, decomposition animations are created using sculpting and blend shapes. No DCC software uses a procedural approach to creating decomposition animations, and the animation's timing is artist-driven rather than from any other source. This project addresses that gap by building a Houdini Digital Asset (HDA) that drives a human anatomical model through the forensic stages of decomposition -fresh, bloat, active decay, advanced decay, and skeletonisation -from a single Days parameter, with independent Temperature and Humidity controls (Figure-1). The system is non-simulated and time-independent: every stage is a pure function of its inputs, evaluated instantly rather than solved frame by frame, which keeps the asset fully scrubbable at the cost of approximating emergent behaviour such as gas pressure rather than physically solving it.

The staged timing algorithm utilises a five-stage weighting system based on Payne's (1965) descriptive model and a thermal summation temperature multiplier. The two are explicitly formulated as equations and verified by direct spreadsheet measurements of the implemented asset itself, rather than by code comments alone or by intended design. The comparison of its speed with the one given by Payne shows that the algorithm works at roughly seven to eight times slower than his pig carrion case. Characterisation of the temperature equation restricts the influence of climate on this gap to no more than about 30%, implying carcass weight and species-proxy problems for pigs relative to humans as the most likely culprits.

This document will describe the science that informed the asset, how the nodes are designed in Houdini, the numerical procedures used to verify the asset after the viewport diagnostics failed to find it, and the technical problems and their solutions. Any current problems in the current version will also be listed. This document will end by defining the border between procedural and human touch (sculpting and textures).

(Figure-1) Body Decomposition Houdini Digital Asset

1. Introduction and Problem Statement

Decomposition is one of the more difficult effects a character or creature pipeline is asked to produce, precisely because it is not one effect but several running at once -volumetric change, surface degradation, discolouration, fluid release, and secondary insect activity -each with its own timing relative to the others. In current production practice, this compound effect is built by hand. A digital sculptor will model the states of death and decompose them into different poses or blend shapes of the rotting body. Then the texture artist paints respective 25 diffuse, displacement, and 3 subsurface maps, each corresponding to one of the states. After that, the technical animator interpolates between the states and adjusts timings to ensure everything works correctly in the engine. Industry training material aimed at working Houdini artists is explicit that, even in pipelines that lean heavily on procedural tooling, this division of labour is still the norm: fine surface sculpting is treated as work "better suited to traditional tools like ZBrush" than to a node graph, with procedural techniques reserved for blocking, scattering and large-scale variation rather than for the specific, biologically motivated surface detail a decomposing body requires (The Gnomon Workshop, 2025). No major DCC package -Houdini included -ships a dedicated decomposition tool, and the timing an artist chooses for a given shot is a directorial decision made by eye rather than a value derived from any external reference. This is an effective creative choice for one hero shot, but it is not scalable. If more than one shot needs to be broken down and/or if the different states need to be believable across different climates or elapsed times, this becomes an increasingly expensive manual process.

A parallel and independent problem exists on the forensic-science side of the same subject matter. That argument depends, however, on three-dimensional documentation actually being available at the scale forensic research requires, and the practical evidence is that it currently is not. Mickleburgh's decomposition-research programme at the Forensic Anthropology Center at Texas State University -one of the more developed examples of this documentation effort, and led by a researcher who is herself a trained 3D modelling and animation specialist - "combines actualistic taphonomic experiments with 3D visualization methods" (Mickleburgh, n.d.), but building each digital replica by hand, bone by bone, and then animating and simulating its change over time is exactly the kind of repeated manual cost the previous paragraph describes, only now paid by researchers rather than by artists. A closely related strand of work -immersive and photorealistic 3D content built for forensic and forensic-adjacent education, including the photogrammetry-based neuroanatomical teaching models evaluated by Trandzhiev et al. (2024) and the virtual crime-scene tools of Mayne and Green (2020) -treats three-dimensional and virtual content as valuable specifically because cadaveric and field-based training material is scarce, expensive and ethically constrained.

These two challenges-industry workflows lacking procedural decomposition tools and research practices constrained by the manual construction and animation of each digital case study: are distinct but share a common obstacle: generating a scientifically timed, decomposed body currently requires repeating the same manual work for each instance. The contribution of this project is a Houdini Digital Asset that eliminates this repetition for a specific use case. The asset drives a human anatomical model through five decomposition stages using a Days parameter, with Temperature_c and Humidity as independent environmental controls. The staged-timing system is mathematically explicit rather than keyframe-based, and its behaviour is verified through direct measurement of the implemented asset. The report is explicit about the asset's limitations: it is not diagnostically accurate, is not intended for courtroom or casework use, and, as detailed in Section 9, its procedural output still requires manual sculpting and texturing to achieve production realism. The statement is carefully defined: an initial process-oriented scientific approach may replace at least the first repetitive step of work required in VFX and forensic visualisation, allowing the artists to focus on polishing the result without having to recreate the whole staged process in the first place.

2. Aim, Objectives and Scope

The overall aim of this project is to develop a Houdini digital asset that can simulate and automate a human anatomy model's decomposition from zero through the forensic periods, using a single, continuous timing parameter, to yield an artist-friendly, technically accurate result without having to hand-model every part.

This aim breaks down into five objectives:

- Translate descriptive forensic staging -principally Payne's (1965) framework -into continuous, blendable numeric weights rather than a set of discrete stage switches, so that transitions read as gradual rather than mechanical.
- Drive the resulting weights through a coherent set of Houdini subsystems covering bloat, tissue slough, desiccation, fracture, organ change, ground staining, insect activity and skeletal exposure, so that all effects stay synchronised to one timing signal.
- Expose environmental control -temperature and humidity -as independent parameters grounded in thermal-summation biology rather than as arbitrary sliders with no basis outside the graph.
- Verify the built asset's actual numeric behaviour, read from the geometry itself, against both its own design intent and the published forensic literature, rather than relying on visual impression alone.
- Document honestly where the asset's behaviour diverges from that design intent and from the literature, rather than presenting only the cases where it agrees.

Three scope boundaries were adopted deliberately during development and are stated here rather than left implicit. First, the system is non-simulated and time-independent: output is a pure function of the Days parameter, with no solver, no cache and no frame dependency. This was chosen over a physically solved approach because it makes the asset fully deterministic and instantly scrubbable -any parameter value can be evaluated and rendered directly, results are identical on every evaluation, and no re-simulation is required when a parameter changes. The cost is that emergent physical behaviours, such as genuine gas pressure, tissue collision or fluid movement, are approximated through attribute-driven displacement rather than solved from first principles. In general, a "delivered range" can only be provided on occasion in conditions representative of the "temperate frame" and may have a restriction to 0-60 days and so represent conditions over the range from fresh until skeletonisation, at which point conditions beyond, such as bleaching and vegetation, are considered not applicable. Third, the asset is tuned to the specific source anatomy supplied with it: region isolation and several spatial masks are keyed to the dimensions of that input mesh, so retargeting to a different character would require re-establishing those groups and re-tuning the masks rather than working automatically.

Crucially, let us be absolutely clear about what the asset does not claim to be: it is not diagnostically reliable; it is not suitable or recommended for court-case or investigative casework; nor does it provide a figure for the post-mortem interval of a real body. The use case is strictly instructional; the asset delivers the process of decomposition but in an easily controlled, repeatable, and ethically unproblematic visualisations format, allowing both student and artist to engage, in some capacity, with a process which has, up until now, relied heavily upon still photography, limited visits to the field, or no access at all.

3. Research: How a Human Body Decomposes

3.1 Descriptive staging and its origins

The dominant descriptive framework in decomposition studies originates with Payne (1965), whose study of baby pig carrion in South Carolina established a six-stage sequence -fresh, bloated, active decay, advanced decay, dry, and remains - defined by observable morphological and entomological criteria rather than by elapsed time. This six-stage vocabulary has since become the common descriptive language of the field, and it is the framework on which this project's five-stage weighting system is directly modelled (Figure-2). A significant point in Payne's analysis that warrants deeper discussion is the time scale: when the environmental conditions were ideal for summer in South Carolina, with insects having unhindered access, he concluded that about 90% of the carcass by mass was gone in six days. Comparisons with insect exclosures revealed that this speed was largely due to insect colonisation of the carcass, not to decay alone (putrefaction). Six days!

(Figure-2) Stages of Body Decomposition

3.2 Climate dependence and the limits of a single reference timeline

Many more studies have now time and again provided evidence showing that Payne's six stages of development do not stay the same length of time, the lengths of the stages being greatly influenced by such factors as temperature, humidity, place of geographical occurrence, climate and presence of associated animals. Griffiths, Krosch and Wright (2020), studying pig carrion in tropical north Queensland, found decomposition proceeding to the dry/remains stage within five days -explicitly faster than every other region in their comparison, including Payne's South Carolina data. Their cross-regional comparison found stage durations varying by two to three days for the fresh stage, one to seven days for bloated, one to eight days for active decay, and five to twenty days for advanced decay. It implies the following methodology:

A single reference timeline, regardless of its documentation quality, can never be taken as the universal truth to measure the speed of a procedure unless the timeline's context is considered.

3.3 Accumulated degree-day frameworks and their contested status

While the qualitative description is provided by the descriptive staging approach the TBS/ADD approach developed by Megyesi et al. (2005) seeks to establish a quantitative connection between the two. TBS scores three body regions -head and neck, trunk, and limbs -each against standardised descriptive categories running from fresh through advanced skeletonisation, sums the three sub-scores into a composite, and converts that composite, via a published regression, into an estimate of accumulated degree-days. This two-step structure is among the most-cited quantitative frameworks in forensic taphonomy and the natural point of comparison for any model, such as this one, that incorporates an explicit temperature parameter. Its status in the literature is nonetheless considerably more contested than its citation count suggests. Moffatt, Simmons and Lynch-Aird (2016) identified rounding inconsistencies, an inappropriate temperature scale and a misapplication of the underlying regression in the original equation, concluding that it could, under certain inputs, produce unusable results including negative ADD estimates, and proposed a corrected equation with a substantially improved fit. Smith, Ehrett, Weisensee and Tica (2023) subsequently published a formal commentary addressing both the original equation and the Moffatt correction. Most significantly, an independent, multi-site validation by Wescott et al. (2018), using cadavers with a known, controlled ADD at three university decomposition research facilities, found that mean ADD estimates from the original regression did not correlate well with the true ADD at any tested interval, and concluded that real decomposition does not, in practice, follow the linear relationship the original method assumes. It is the purpose of this literature to show that scoring based on ADDs is an area of active debate and development, so much so that considering the 2005 formula as the ultimate benchmark will only serve to reveal how naïve such a presumption is.

3.4 Entomological succession: body-clock and insect-clock measures

There is an additional, somewhat overlapping method that utilises succession: the appearance and disappearance of distinct groups of insects (largely blow-flies and, finally, beetles) over time provide a "forensic clock". This measure is distinct from the ADD measure of Section 3.3: a body's decomposition state and a colonising larva's developmental stage can diverge, for instance following a colonisation delay. This project's insect-activity gate does not distinguish between the two clocks, deriving insect activity directly from the same stage weights that drive the body's visual state, a simplification that Section 8 records. Two recent studies from the Forensic Anthropology Centre directly inform this system. For humans, we already know from multiple-season human experiments that there's much variation even in exposure to similar weather conditions from the earliest history until after colonialism has happened (2). Therefore, I assume that time to colonisation may represent a biological variable rather than a consequence of climate. Furthermore, according to Owings et al. (2022), in one experiment, the first oviposition occurred only 115 days after deposition, and re-colonisation took place much later than the feeding stage ended:something that can never be represented by any monotonic activity function, including the current one.

3.5 Decomposition chemistry and soil interaction

The phenomena of purge-fluid ejection and ground staining modeled in the present study have their basis in decomposition chemistry literature, mainly in the work of Vass et al. (1992, 2002), who defined the composition of volatile fatty acids and the alteration in the soil solution caused as the decomposition fluid permeates the soil layer underneath the body due to decomposition, as well as Campobasso, Di Vella, and Introna (2001), who describe the environmental factors influencing the rate of decomposition and colonization by insects. This research shows that fluid ejection is an important, nonaccidental process and an independently identified chemical event, occurring in conjunction with abdominal rupture.

3.6 The pig-proxy problem

Both of the calendar-day benchmarks drawn on in this report -Payne (1965) and Griffiths et al. (2020) -are pig-carcass studies, not human decomposition studies (Figure-2). This is worth stating separately from the climate-dependence issue above, because it introduces a distinct source of uncertainty. Domestic pigs (Sus scrofa) have long been the default proxy species in forensic taphonomy, favoured for their physiological and anatomical similarity to humans combined with the practical difficulty of obtaining human cadavers for controlled experimental research. Direct comparative research, however, finds the proxy relationship holds less cleanly than its widespread use suggests. Figure 2: TBS of 17 and 22 pig and human specimens with each comparison under paired field conditions. The comparison showed an overall significant difference, with no pattern that fit the well-established regression line for either TBS or ADD (223,234) for the pig post-mortem intervals. A broader review by Matuszewski, Hall, Moreau, Schoenly, Tarone and Villet (2020) concludes that differences in decomposition rate, pattern and scavenging between pigs and humans are real and documented, while noting that pig-based studies remain, for reasons of access and replicability, the primary epistemic source of forensic taphonomy knowledge. This question of species is separate from the question of body mass, addressed directly in Section 6.

3.7 What actually happens across the modelled 60-day range

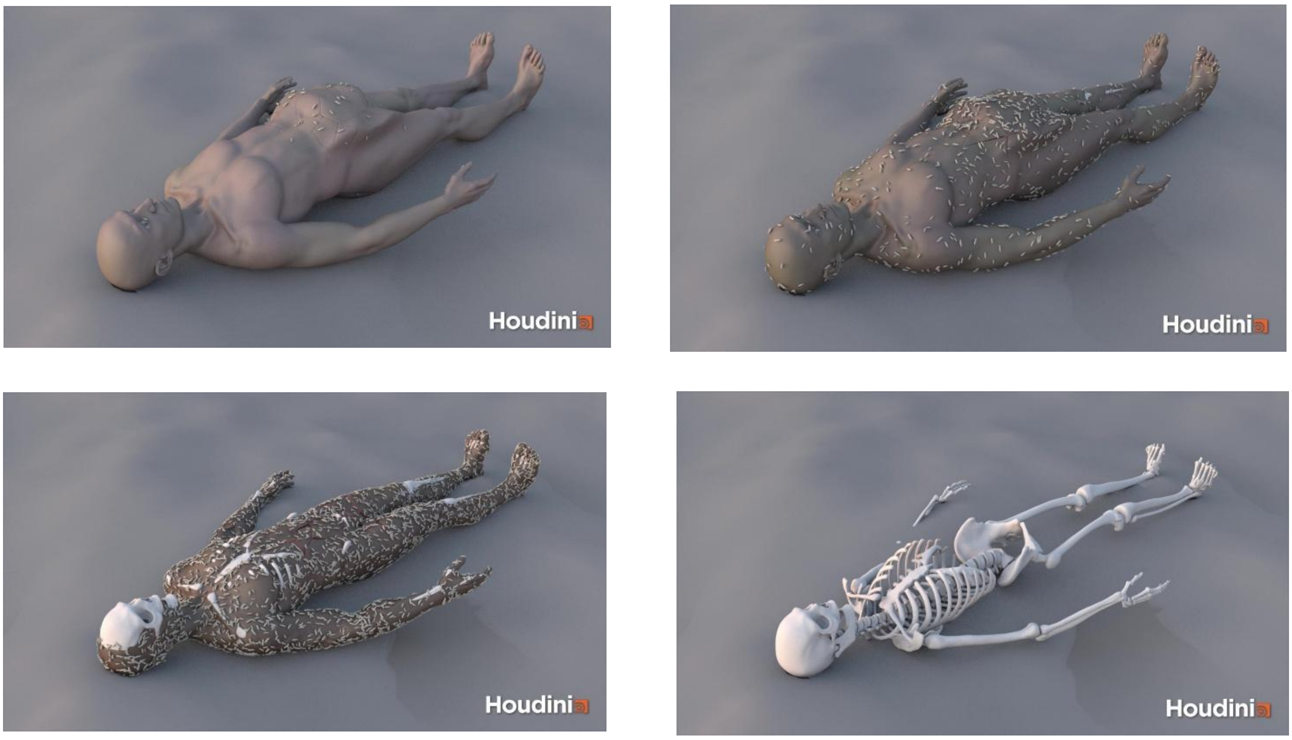

(Figure-3) HDA-generated decomposition model

Reduced to a single narrative rather than a citation list, the research above describes a recognisable day-by-day sequence, and it is this sequence the Houdini asset is built to reproduce. In the fresh stage, immediately after death, the body shows no external sign of decomposition to the untrained eye: internal autolysis and the earliest bacterial activity have begun, but skin colour, volume and surface texture remain close to living appearance, and this is the state the model returns at Days close to zero. As anaerobic gut bacteria -principally Clostridium and Bacteroides species -begin fermentative metabolism, gas accumulates fastest where bacterial load is greatest, and the abdomen distends first and furthest; this is the bloat stage, the point at which the body becomes visually unmistakable as decomposing. Distension continues until intra-abdominal pressure exceeds the tensile strength of the abdominal wall, at which point rupture releases the trapped gas and expels purge fluid into the surrounding substrate, and it is this rupture -not an arbitrary elapsed time -that the model treats as the trigger for ground staining. Active decay. The body collapses due to gas release; soft tissues are degraded relatively quickly by bacterial action and, where they occur, by feeding larvae; mass loss is at its maximum of the entire sequence. As accessible soft tissue is exhausted, the process moves into advanced decay, in which remaining tissue desiccates rather than actively decomposing, skin darkens, dries and begins to detach from the underlying structure, and skeletal elements start to become visible at the sites where soft-tissue coverage was always thinnest -skull, ribcage, hands and feet. In the final, skeletal stage modelled here, exposed bone dominates the visible surface, remaining soft tissue is limited to protected or deep sites, and the body has reached the functional endpoint of the 0–60 day range this asset represents. Insect activity, represented separately in the model, is not a background detail across this sequence but one of its principal drivers: colonisation follows shortly after death, larval mass and activity peak during active decay, and larvae disperse as the advanced-decay stage completes -the successional pattern Section 3.4 describes, and the pattern this project's insect-activity gate is built to track, if only directionally rather than to the accumulated-thermal precision the entomological literature itself works to (Figure-3).

4. From Biology to Mathematics

The preceding section describes decomposition as forensic taphonomy observes it: a qualitative, staged framework built from direct observation, in which a body is placed into one of a small number of descriptive categories. A Houdini node graph cannot consume that framework directly -it needs a continuous, computable signal to blend, mask, and drive other systems. This section translates the observational staging of Section 3 into continuous weighting functions that a procedural graph can use directly, and that translation -not any single visual effect built on top of it -is the core technical contribution of this project's timing system.

4.1 Smooth interpolation and the stage partition

The transition between all stages can be done using the cubic Hermite interpolator known as smooth step, which is available in Houdini as smooth(a, b, x). Using the normalised parameter $\tau = \text{clamp}((x - a) / (b - a), 0, 1)$, the smooth step interpolation takes the form $S(x; a, b) = \tau^2(3 - 2\tau)$. It is a C^1-continuous function such that $S = 0$ and $S' = 0$ at $x = a$, and $S = 1$ and $S' = 0$ at $x = b$ (Lengyel, 2012). The fact that the first derivative of this function vanishes at both ends is important: when the transition is made using such an interpolation, it will neither start nor end with the sudden change of the rate, which would have looked as a mechanical jump between the stages had it been a linear interpolation.

The four cumulative ramps defined on an effective time e to be introduced in the next subsection each represent a stage boundary: S = S(e; 0, 10), S = S(e; 5, 19), S = S(e; 15, 29), S = S(e; 28, 52). The five-stage weights are the successive differences of those cumulative ramps: w = 1 S, w = S S, w = S S, w = S S, w = S.It is easily verified that this construction forms a partition of unity: the sum telescopes to $\Sigma w_k = 1$ identically for any e, and for any choice of ramp ranges. This feature is used in combination with five individually generated anatomical representations, without requiring any normalisation and without generating residuals over time. This is the desired construction; differences in the weights used from this construction can be seen in Section 7, and these differences are not corrected in this discussion.

Note that these ramp intervals shown are in the output, and not solely defined in comments, which is of some consequence given the problems with diagnostic reliability described in Section 7. If the interpolant for the fourth ramp interval is evaluated at an effective day of 31.5, then = 0.145833, and S = 0.05759910 when the measured w was 0.057599; if evaluated at an effective day of 51.0, then = 0.958333, and S = 0.99493634 when the measured 0.994936. Note that 1-S also corresponds to w, and has values of 0.94240090 and 0.00506366, in good agreement with the measured values of 0.942401 and 0.00506365. It is good that at both points, and for both weights, there is agreement to the full level of precision available, indicating the ramp interval and not simply one intersection of two ramps.

4.2 Thermal summation and the temperature term

The biological principle underlying every temperature-driven forensic timing model is that the processes governing decomposition -bacterial metabolism, enzymatic autolysis, and the development of colonising insect larvae -are carried out by poikilotherms whose rate scales with ambient temperature above a lower developmental threshold T_0, below which activity effectively ceases. Temperature and biological development over biologically meaningful temperatures are generally taken to be linearly related such that growth rate toward an adult is measured byr(T)= (T T)/K forT T whereK is the thermal constant, expressed in degree-days and the process completes when integral from 0 tot off T(t) T dt= K. Left side of the first equation is the accumulated degree-day measure in Section 3.3. The identical integral calculated in degree-hours with species- and instar specific threshold is the standard used in forensic entomology to age larvae and it is the formal justification for the two-clock distinction between these measurements made in Section 3.4: these measures have the same form and are integrated against different subjects and constants. The two critical thresholds are biologically relevant, and this model demonstrates one of them: bacteria responsible for putrefaction are essentially rendered inactive at 4°C, which is why the temperature of mortuary cooling is kept at about this level, whereas fly larvae development has a lower critical threshold at 10°C.

The resulting multiplier is a piecewise-linear function expressed through

$m(T) = 1.05\ (T - 4)/16$ if $4 \leq T \leq 20$, and

$m(T) = 1.05 + 0.0225\ (T - 20)$ if $20 < T \leq 40$,

$e = D \cdot m(T) \cdot h(H)$,

and the clamp operation is performed such that $m(T) = 0$ if $T < 4$°C and $m(T) = 1.5$ if $T > 40$°C. The variable responsible for effective time in the stage-partitioning scheme is

where D is the number of elapsed days, and h(H) is the humidity component with value 1 at normal level. The temperature term is confirmed by measurement at three settings, returning 1.050, 1.275 and 1.500 at 20, 30 and 40°C respectively, and the effective-time variable is confirmed strictly proportional to D with no additive offset at two values of D. The lower segment has the exact form of the thermal-summation rate law above with $T_0 = 4$, which is what makes the degree-day conversion exact rather than approximate in that regime: at constant temperature, $e = D \cdot 1.05(T - 4)/16$, so $ADD_4 = 15.238 \cdot e$, where ADD_4 denotes accumulated degree-days above a 4°C base. This is confirmed against measured output -at D = 30 and T = 20°C, degree-days on a 4°C base are 480, and the measured e of 31.5 returns 480.0 exactly. Above 20°C the slope falls from 0.065625 to 0.0225 per degree, the upper segment departs from the biological rate law, and the degree-day conversion no longer applies. That departure is where the model parts company with its own biological rationale, and its cost is quantified in Section 7.

4.3 Tissue retention, skin loss, and bloat

The desiccation/sagging that occurs is approximated by a signed distance field derived from the skeleton. The values inside the bone are set to -1 and 1, pointing outwards from the bone. The vertices on the skin surface are moved in the direction of the gradient, with the magnitude proportional to the late-stage weights, causing a localised collapse of the tissues towards the underlying bone rather than the centroid of the entire body. The motivation for tying retention to tissue depth is that water escapes through the surface; thus, the rate of desiccation is proportional to the ratio of tissue depth to surface area. This results in faster desiccation and skin loss on the surfaces of the skull, rib cage, and pelvis compared with the deeper areas of the limbs and the lower

Skin removal is performed using a stochastic procedure we call stochastic thresholding. The removal of a primitive i is determined by a value of removal threshold, which is given by a remove_threshold,i=0.15+0.80 ·(p), where ,i is the spatial noise field ranging from [0,1] while our global gate is determined by g =clamp(fit(w, 0.5, 1.0, 0, 0.3) + w,0,1) and it monotonically increases in the final stage. Primitive i is deleted wheng >.

Given the value of the removal threshold of primitives and the monotonicity of the gate, this procedure is not irreversible.

In case that this spatial noise field is drawn uniformly, then the expected amount of skin to be removed will beCg=1−clamp((g−0.15)/0.80,0,1). Therefore, wheng=0.95all the skin would be removed.

Bloat is driven by the same anaerobic gut-flora fermentation described in Section 3.7, and the model applies its largest regional volume gain to the abdomen for the same reason production is greatest there. The abdominal mask A = S(n_h; 0.32, 0.45) · [1 − S(n_h; 0.50, 0.62)] · [1 − S(d⊥; 0.105, 0.15)], for normalised head-to-foot coordinate n_h and lateral distance d⊥ from the midline, localises both the distension and the tear density that later seeds the fracture system, and rupture -rather than an arbitrary elapsed time -is the event that terminates the bloat stage and gates the onset of ground staining.

5. Implementation in Houdini

Section 4's equations are computed in a single node, referred to throughout development as BRAIN. It reads three user-exposed parameters -Days (integer, 0–60), Temperature_c (integer, 0–40) and Humidity (float, 0–1) - evaluates the effective-time variable and, from it, the five stage weights. Each weight is then read downstream by multiple independent effect nodes, so a single centrally computed timing signal drives skin bloating, tissue removal, discolouration, insect activity and skeletal exposure coherently, rather than each effect reimplementing its own timing logic. This blend structure, rather than a discrete stage switch, is what allows smooth visual transitions between stages instead of an abrupt snap. Below, each subsystem is covered in turn, stating what node or node group implements it, why that approach was chosen over the alternatives, and how it is driven by the timing model.

5.1 Region separation and volumetric representation

At the right, Anatomy graph enters this, and the whole piece is separated by region using, respectively, keepskin, keep skeleton, keep eyes, and keep other, partitioning the 4 kinds of tissues by an @regionid attribute; connectivity1 handles individual- piece identity so they may be shattered later, etc. Next, SKELETON SDF is the skeletal geometry translated into a signed distance field,, which is then exported as SKELETON VDB_OUT to the balance of the graph. We must transform the skeleton into a signed distance volume for this to work in the desiccation algorithm and skin-bone clamp in Section 5.4; otherwise, skin-body interaction requires an extremely slow nearest-neighbour query into a large set of polygons, or it simply won't give well-defined normal directions for moving each skin point towards the nearest boundary in the rest of the system.

5.2 Soft-tissue systems

BLOAT_SKIN drives abdominal and torso volume increase as a function of w_2 and the abdominal mask of Section 4.3. DESICCATIONSHRINK is done away with the skeleton signed distance field in favour of the body centroid, which fixed a prior bug that caused the skin to blow up at a single point rather than simply sink into the structure closest to it. Likewise a gravity sag is applied which uses the same field to model gravity making the surface flatten on the relative closest underlying structure not an absolute floor, and excluding skinny leg extremities that was encountered during development from being similarly attracted so they appear to pull away underneath. DECOMPLAYERS and SKIN_SLOUGH are derived from the previously established statistical distribution used in 4.3

5.3 Fracture, wound and insect systems

This is modelled as a localized abdominal wound created using Voronoi Fracture rather than displacement as Fracture is discrete yielding separate shells which can be individually tracked and contracted by displacement-only.tear_points scatters seed points within the tear-density field of Section 4.3, tear_points_jitter randomises them, and skin_fracture (Voronoi Fracture) produces the fractured skin shells; a for-loop between piece_begin and shrink_piece and piece_end then contracts individual fragments as decomposition proceeds. Activity of the flies is expressed two ways. The parameter ORGAN_COLOR and the colour-spacee map also darken an andd desaturate the shadin, surrounding the wound at scales w + ,w asa function to be interpreted as an activity indicato,r where actual flies would notbe be resolved at this distance by the camera lens.

A geometry-based chain - MAGGOT_TEMPLATE → POLYFILL1 → MOUNTAIN1 → POLYBEVEL1 → MAGGOT_TAPER → MAGGOT_DENSITY → MAGGOT_SCATTER → MAGGOT_VARIANCE → INSECT_ACTIVITY → MAGGOTS_FINAL :

builds an instanced larval geometry and scatters it onto the wound surface, with density driven by the product of the tear-density field and the same stage weighting. Each instance's long axis is aligned to the local surface tangent rather than the surface normal, a distinction that matters in practice: aligning to the normal produced every instance standing upright rather than lying along the wound, which was one of several cases in this project where a physically small implementation detail had a disproportionate effect on whether the result read as correct.

5.4 Organ, fluid and settling systems

ORGANCOLOR: Organ internal colour. ORGANSLOUGH: How organs decay and are lost due to the fact that fracture cracks. PURGEPOOL runs on purgepool_grid and causes under-the-body decomposed-fluid stain. Stain occurs when the belly gives up the ghost, turning on over abdominal deformation and cumulating staining over time, as suggested by 3.5, 4.3, etc, so that staining once begun persists. PIECE_HEIGHTS records per-piece elevation, and GRAVITY_COLLAPSE applies post-skeletonisation settling as vertical displacement once all other subsystems have merged. settled_skeleton isolates the settled bone by region, vdb_settled_skeleton rebuilds a signed distance field from it at 0.004 voxel size, and a point wrangle, SKIN_BONE_CLAMP, uses that field to hold skin outside bone by displacing any skin point found inside the bone surface back out along the field gradient with a 5 mm clearance margin. merge_all combines every system into the asset's single output.

5.5 Representative VEX excerpts

The following two wrangles illustrate how the mathematical formulation of Section 4 is expressed directly in VEX rather than remaining only a design document. The first implements the skin–bone clamp of Section 5.4, projecting any skin point found inside the settled skeleton's signed distance field back outside it along the field gradient:

```
// SKIN_BONE_CLAMP -point wrangle, geometry at input 0, VDB volume at input 1
float margin = 0.005; // 5 mm clearance
float phi = volumesample(1, "surface", @P);
if (phi < margin) {
    vector grad = normalize(volumegradient(1, "surface", @P));
    @P += grad * (margin - phi);
}
```

The second implements the stochastic skin-removal law of Section 4.3, reading a per-primitive threshold noise attribute and the global gate g computed upstream in BRAIN, and deleting primitives whose threshold has been exceeded:

```
// SKIN_SLOUGH -primitive wrangle
float theta = 0.15 + 0.80 * chf("noise_seed") * fit01(rand(@primnum), 0, 1);
float gate  = clamp(fit(chf("w4"), 0.5, 1.0, 0, 0.3) + chf("w5"), 0, 1);
if (gate > theta) {
    removeprim(0, @primnum, 1);
}
```

Both wrangles are written to read their driving values -the volume gradient in the first case, the global gate in the second -from upstream nodes rather than recomputing them locally, which keeps the whole graph consistent with the single-source-of-truth structure described at the start of this section: if the timing model in BRAIN changes, every downstream system that reads its weights changes with it, without needing to be independently re-authored.

The delivered asset's render output was produced by driving Days from the frame number across a 60-frame sequence covering the full 0–60 day range, which is possible precisely because the system is non-simulated: there is no solver to step and no cache to invalidate, so any subset of the range can be re-rendered independently of any other. This scrubbability, more than any single visual effect described above, is the practical payoff of the architectural decision made in Section 2 to keep the system a pure function of its inputs.

6. Verification and Results

6.1 Verification method

Pipeline processes based on procedures are prone to a certain form of error: the final rendering may look fine despite being wrong due to the data used. The reason is that unconverged renderings, viewport shading, and the similarity of the results make the logic error invisible. This was encountered repeatedly during development, and traced in each case to a conclusion drawn from how a render or viewport looked rather than from the attribute values actually driving it. The practice adopted in response, and applied to every quantitative claim in this report, was to treat any visual judgement as provisional until confirmed by reading the relevant attribute from the geometry spreadsheet at a known parameter value -the specific attribute, the specific Days value it was read at, and the specific number returned. That protocol, described in more detail in Section 7, is the source of every measured (Figure-4) reported below.

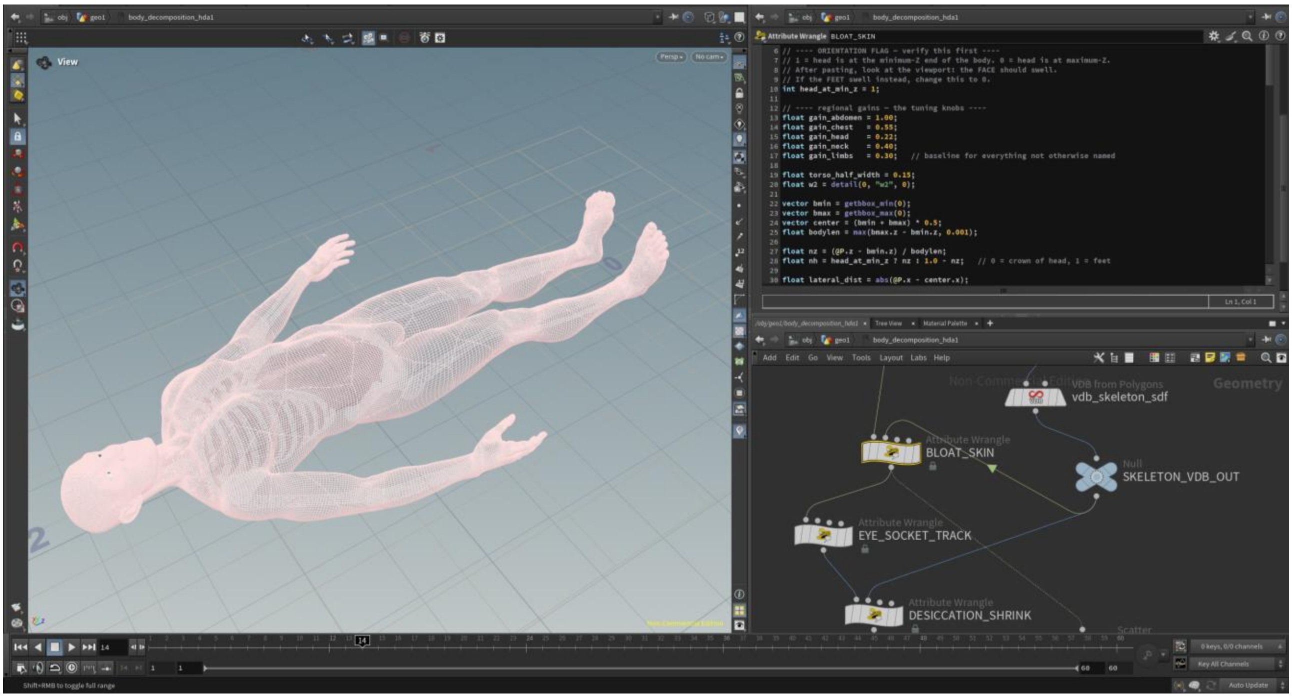

(Figure-4) Bloating system through Attribute Wrangle coding

6.2 Stage-crossover comparison against Payne (1965)

The model's stage-crossover points were established two ways: from the design values documented in code comments within BRAIN, and from direct spreadsheet reads of the actual w1–w5 values at a baseline test condition of Temperature_c = 20, Humidity = 0.5. The two agree, confirming the implementation has not drifted from its design during development -a real risk in any iteratively built procedural pipeline, and precisely the kind of claim this section's method holds should never be accepted without numeric confirmation

Stage	Design intent (Day)	Confirmed empirical crossover (Day)
Fresh (w_1 dominant)	0–3	$w_1 = 0$ by Day 10 (endpoint below Day 10 not directly tested)
Bloat (w_2 dominant)	3–12, peak ~7–8	w_2 dominant at Day 10 ($w_2 = 0.658$); w_3 overtakes by Day 15
Active decay (w_3 dominant)	12–22	dominant Day 13–21; w_3/w_4 crossover at Day 21 (both 0.485/0.515)
Advanced decay (w_4 dominant)	22–40	dominant Day 21–32 ($w_4 = 0.862$–0.959 across samples)
Skeletal (w_5 dominant)	40+	w_5 rising by Day 30 (0.058), 0.302 by Day 35; full reveal by Day 45

Against this, Payne's own reported finding is that under full insect access and favourable summer temperature, 90% of carcass mass was removed within six days. This model's skin persists in substantial form through approximately Day 30–35, with full skeletal exposure not confirmed until Day 45 -roughly seven to eight times slower than Payne's benchmark. This discrepancy is stated plainly rather than minimised. Three explanations were considered, are not mutually exclusive, and are not equally well evidenced. The most substantial, on the evidence assembled, is a difference in body mass: Payne's study is of a neonate pig, while the anatomical model here represents an adult human, and neither mass is established in this report, so the ratio between them is unquantified. What is well evidenced is the direction and existence of a mass effect: Sutherland et al. (2013), comparing pig carcasses under 35 kg against carcasses of 60–90 kg under matched temperate conditions, found the smaller decomposed 2.82 times faster overall, and Matuszewski et al. (2014), across four mass bands, likewise found mass to exert significant effects, attributing the mechanism to competition within a multi-guild insect assemblage rather than to any physical property of the carcass itself. The second explanation, climate, has been tested directly and substantially ruled out as a full explanation: the temperature multiplier is clamped at 1.5, so the fastest timeline the model can produce at any temperature is its baseline divided by 1.5, placing full skeletal exposure no earlier than approximately Day 30 against Payne's six days -temperature-matching reduces the discrepancy to roughly fivefold and cannot close it, so climate accounts for at most about thirty per cent of the gap. The third, the species-proxy uncertainty of Section 3.6, applies to Payne's own benchmark independently of both mass and climate and has not been disentangled from them here.

6.3 Internal-arithmetic verification

Quantity	Value	How confirmed
temp_mult at 20 / 30 / 40°C	1.050 / 1.275 / 1.500	Direct reading, three settings
eff_days vs Days	Proportional, no offset	Two values
ADD_4 at baseline	480	Two independent routes
Stage weights at e = 31.5	w_4 0.942401, w_5 0.057599	Geometry spreadsheet
Stage weights at e = 51.0	w_4 0.00506365, w_5 0.994936	Geometry spreadsheet
Weight sum at e = 9.45	1.00209 (should be 1.0)	Partition overshoot -see Section 7

These figures matter beyond their individual content, because the crossover table above rests substantially on a single measured coincidence -the w_3/w_4 crossover at Day 21 against a predicted 21.0 -and one crossover point could in principle be reproduced by a ramp pair that was wrong but similarly shaped. Confirming both weights simultaneously at two widely separated points constrains the shape of the ramps themselves, not merely the location of one intersection, which is why the ramp-interval recovery reported in Section 4.1 is treated in this report as the stronger result of the two.

6.4 A negative result: bounding the temperature contribution

This test was determined as the most pressing remaining verification, and the highest priority outstanding calculation against the experiment from an earlier date due to the direct calculation against Payne's field conditions once matched by temperature. This work has now been superseded by an even more definitive, even simpler measurement by entirely foregoing the recovery of Payne's actual field conditions temperature. Due to the multiplier of 1.5 that is the absolute upper bound on the temperature term, a model that matches Payne's field setting to within ~1/5 is not possible, under any temperature setting of the model. This is stated here as a finding, as it resolves the need for a further run that would otherwise have been deferred.

7. Errors, Trial and Error

In the text that follows, the process of technical failings in the build that were encountered in observations to a measured conclusion, to taking action to finally achieve a verified result, is given under a standard framework, and this continues throughout, even when the issues were from an ongoing failure and were included.

7.1 Skeletal protrusion through intact skin

Observed: Bones appeared through intact skin on the skull, rib cage, hands, and feet during the mid-decomposition phase. Measurement: Avoiding the use of GRAVITY_COLLAPSE allowed us to conclude that the fault was in that node specifically, rather than either skin or bone. Conclusion: In the settlement process, bones are moved in rigid translation (Figure-5), so their dimensions are preserved exactly, whereas soft tissues are compressed proportionally to their height; in the case where soft tissue is thin, proportionate compression causes skin to be pushed through the incompressible bone underneath it. What was done: Instead of fixing the settlement algorithm, which worked perfectly fine by itself, we introduced an additional post-processing stage which consists of isolating regions of the settled skeleton, converting them into a signed distance field with 0.004 voxel sizes, and displacing points of skin that lay inside the skeleton surface with a point wrangle (SKIN_BONE_CLAMP) in the direction of increasing values of the distance field with a 5 mm clearance from it. Verification: Output render confirmed no bones were protruding from the skin anywhere in the parameter space. Tradeoff: Explicitly stated instead of being hidden -this is a workaround rather than a fix to the core problem. The problem in this case is that the skeleton and the skin were created independently of one another and never registered. Thus, the point wrangle clamps the skin but does not fix its registration, and it keeps the skeleton and skin thicknesses at the thin parts approximately correct. An alternative solution of uniformly reducing the skeleton by 4% about its own centre was implemented and verified, but is not included in the submitted build.

(Figure-5) Skeleton dragging error

7.2 Diagnostic unreliability and the numeric-verification protocol

Observed: an unusually high proportion of early diagnoses drawn from visual inspection proved wrong on closer examination. Measured: three specific false alarms accounted for a substantial share of early development time - interior wireframe display drawing bone edges through skin and being read as bone protrusion where none existed; displacement in the 45–100 mm range being effectively invisible in wireframe shading and being read as a system doing nothing; and apparent skeletal visibility through intact tissue that final rendering showed was not actually present. Finished: The disparity between the appearance of the correct and incorrect states on this asset is often smaller than the gap between the viewport and the render, leading to unreliable viewport diagnosis across the board in this project, not just in the unfortunate exceptions. Done: a four-rule protocol was adopted and applied for the remainder of the project -no diagnosis without a number, drawn from geometry spreadsheet values or node info-panel readings rather than a viewport image; judge visual results in rendered output only, treating the viewport as a navigation tool rather than an assessment tool; verify the spreadsheet's sort state before reading it, since a sorted column makes every other column a non-random sample, which itself produced several further incorrect conclusions before the rule was adopted; and confirm every VEX paste, since code was silently appended rather than replaced on at least five occasions, producing duplicate variable declarations. Verified: the crossover and internal-arithmetic figures in Section 6 are the direct product of this protocol, and the protocol itself is treated in this report as one of the project's concrete deliverables rather than only as process.

7.3 Faults still live in the submitted build: (Figure-6)

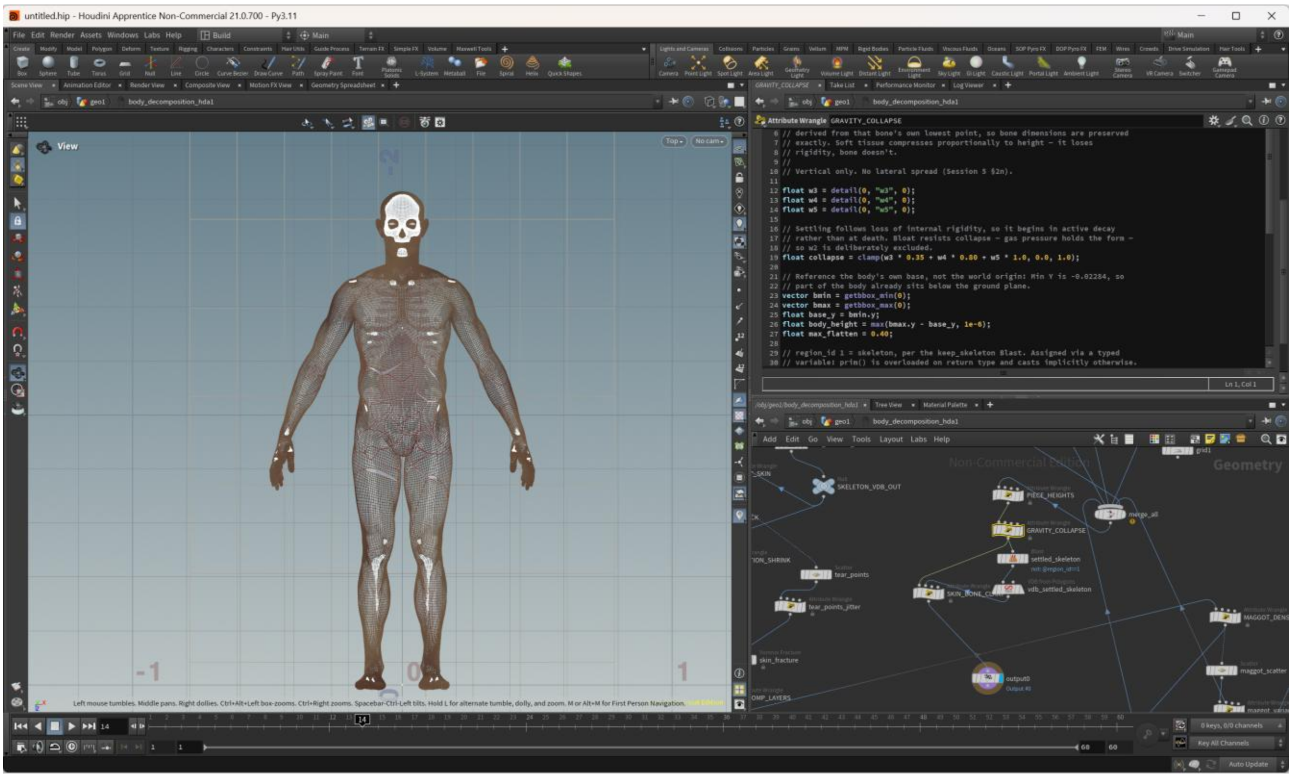

(Figure-6) Faults still live in the submitted HDA

Several issues identified during development are not corrected in body_decomp_18.hipnc, and are recorded here rather than allowed to remain implicit in the results of Section 6:

- Skin–skeleton registration is uncorrected -approximately 1.4 mm clearance at the cranial vault against a real scalp thickness of 5–7 mm. The corrective rescales described in Section 7.1 were developed and verified but are not in this build; their symptom is suppressed by SKIN_BONE_CLAMP, but the cause is unaddressed.

- The weights per stage don't sum up to precisely one – found to be 1.00209 at day 9.45 on effective day due to the ramps in section 4.1 overlapping instead of tiling as planned in the equation; consequence w is nowhere near 1.0 (peak is near 0.79) so the bloat system has never actually run as powerfully as it was optimised for.

- Skeletal exposure is bilaterally symmetric -the lateral-position term intended to drive asymmetry was scaled as though spanning a unit range when its measured values are of order 0.001, so it evaluates to approximately zero. The one-line correction is identified but not implemented.
- Insect activity is deterministic -no variance, delay, or re-colonisation mechanism, despite the literature reviewed in Section 3.4 documenting all three in real donor data.
- Settling is translational only -no rotation about joints, no lateral spreading, no inter-bone collision.

8. Discussion

As indicated in 6, a pertinent question is what purpose such a system would serve, especially given the rate variations and technical problems described in 7.

The literature reviewed in Section 1 and Section 3.7 suggests a clear and, this report argues, appropriate answer. Mayne and Green (2020), Jani and Johnson (2021) and Trandzhiev et al. (2024) together document a well-established pattern: three-dimensional visualisation is adopted in forensic and anatomical education specifically because physical, field-based and cadaveric resources are expensive, geographically restricted, and available in far smaller quantity than the number of students who could benefit from them -and such visualisations are well received and educationally valuable without ever needing to function as diagnostic-grade replacements for the real specimen. This asset is best understood in the same terms. It is not a diagnostic instrument and makes no claim to estimate a real postmortem interval. It is a controllable, repeatable, ethically unproblematic visualisation of a process students or artists would otherwise encounter only through static photographs, a small number of field visits, or not at all.

This framing carries an ethical dimension that warrants explicit statement, since the subject matter concerns human death. A procedurally generated visualisation, unlike photographic material of real decomposed remains, does not reproduce an identifiable individual’s death and does not carry the same risk of distressing a bereaved family or violating the dignity extended to donated remains. This is a genuine advantage over training material drawn from real case photography, and it is consistent with the pattern noted throughout Section 1 and Section 3.7, in which visualisation technologies are valued partly because they reduce reliance on scarce and ethically sensitive specimens. This does nothing to remove the necessity of content warnings and confined application in a pedagogical context, nor does it relieve any of the accuracy requirements detailed over the course of this report; a device that is ethically designed and implemented but silently misrepresents what it's being used to picture would still be a deficient tool, and the corrective work noted in Section 9 is of value only because a device that misrepresents even the relative speed or ordering of decomposition has the potential to teach an intuited false-which a student could extrapolate beyond this device's limitations.

9. Future Development

Ordered by expected value relative to effort, the following items follow directly from the limitations recorded in Sections 6 and 7.

1. Register the source anatomy. The uniform skeletal reduction already developed and verified during this project (Section 7.1) should be carried into the working build. This removes the root cause that

SKIN_BONE_CLAMP currently only masks, and would allow the clamp margin to be reduced or the clamp removed entirely.

2. Fix the stage-weight partition. Applying successive differences to be directly in the exact way which was intended in 4.1 below would also make w fully recovered for bloat to operate with the appropriate tuned parameters for the first time. This would shift all of the stage-end values stated in 6. And would necessitate the timing investigation to be repeated from start to end.

3. Normalise the lateral asymmetry term. A one-line change against the body's actual half-width, expected to produce left–right variation in skeletal exposure without any change to input geometry -the cheapest item on this list relative to its visual payoff.

4. Physically based gas pressure. Replacing the attribute-driven bloat of Section 4.3 with a solved internal-pressure object would produce genuine cavity inflation, self-collision and rupture behaviour rather than displacement along surface normals. This would reintroduce a frame dependency and caching requirement, so it is best implemented as an optional high-fidelity mode alongside the deterministic path rather than as its replacement, preserving the scrubbability that is currently the asset's main workflow advantage.

5. Re-derive climate response from thermal summation. The temperature term under-responds relative to the model's own sub-20°C formulation by roughly a third, and relative to the wider literature by a considerably larger margin -the single clearest instance in this project of the model teaching a wrong intuition rather than merely an incomplete one, and worth correcting for that reason alone.

6. Extend the range beyond 60 days. Later-stage phenomena -bone bleaching, vegetative colonisation, long-term skeletal weathering -would extend the asset's usefulness toward archaeological as well as forensic timescales.

7. Generalise the input. Replacing hardcoded region groups and dimension-keyed masks with an automated region detection or user tagging step would make the asset retargetable to arbitrary character meshes, which is currently the main barrier to any reuse of this tool beyond the specific source anatomy it was tuned to.

8. Rig-driven rigor mortis. Joint stiffness driven by the timing model would introduce postural changes in the early stages, which are currently represented by surface and colour changes alone.

9.1 What still needs an artist's hand

None of the items above address a limitation that the earlier sections of this report have not already stated plainly, and it is worth closing this section with one more that has not yet been stated: this project cannot, and does not claim to, produce a fully production-realistic decomposition sequence by procedural means alone. What the asset delivers is correct staging, plausible large-scale form, and behaviour that is at least directionally grounded in the literature reviewed in Section 3 -the skeleton of a shot, not the finished shot. Two categories of work sit outside what a node graph of this kind can do well. The first is texture: the diffuse, roughness, subsurface-scattering and displacement detail that actually reads as decomposing skin at close camera range -mottling, localised discolouration, moisture sheen, insect damage at a scale finer than the geometric wound this asset produces -is a hand-painted or scan-derived texturing problem, not a procedural-shading one, and the asset as delivered uses the unmodified diffuse textures supplied with the source anatomy rather than decomposition-specific maps. The second one comprises carved features in areas that the procedural method deliberately ignores, such as the subtleties of wrinkling and localised tearing, asymmetric damage caused by environmental contact or scavenging, and the single flaw that lends authenticity through its lack of systematicity. And this matches industry practice which already draws the kind of distinction referred to and relied upon in Section 1 - that is, procedural tooling is suited for masking (blocking), major variation, and globally constant (i.e. procedural) variation (rule based) applied to the whole mesh, whilst procedural-based final pass surface specific realism is - and almost certain to remain - a postprocess added via manual sculpting and texturing. What we are really claiming, honestly, is that we have automated the first part, not the latter.

10. Conclusion

This project set out to address a gap stated plainly in Section 1: decomposition sequences are conventionally hand-sculpted, no major DCC package offers a procedural alternative, and the resulting timing is art-directed rather than derived from any external reference. The delivered Houdini Digital Asset closes part of that gap. It drives a human anatomical model through five decomposition stages from a single Days parameter, with independent temperature and humidity controls, using a staged-timing model whose mathematical form is stated explicitly as a set of equations rather than implied by keyframes, and whose behaviour has been measured -not merely designed -against both its own intended form and the forensic literature reviewed in Section 3.

What has been measured supports a real, though narrow and explicitly bounded, claim of forensic grounding. 1 'model's stage vocabulary and sequencing can be seen to have their ultimate source in Payne's (1965) schedule; its insect activity and purge fluid dynamics' behaviour parallel those implied in the entomology and decomposition chemistry literature discussed in sections 3.4 and 3.5; and its intrinsic calculation algorithm for duration ('temperature multiplier', degree-day multiplier, ramp interval' intervals underlying the stage partition -has been recovered from the asset’s own output and confirmed to five and six significant figures at widely separated points, rather than merely asserted from code comments.

The technical record is reported with the same standard applied to its results. The project experienced a lost development branch, a period of structurally unreliable viewport-based diagnosis, and a specific settling defect that required a corrective, rather than a root-cause, fix; the practices adopted in response to each are documented in Section 7 as concrete outcomes of the project in their own right. A number of faults -an unregistered source anatomy, a stage-weight partition that does not sum exactly to unity, a symmetric skeletal-exposure pattern, and a deterministic insect system -remain live in the submitted build and are stated as such rather than as resolved.

In conclusion, this asset is not, and does not purport to be, a finished, production-realistic decomposition pipeline. It provides correct staging and plausible large-scale form based on scientifically referenced foundations, and it eliminates the repeated first-pass manual effort required in both current VFX practice and forensic visualisation research. However, it does not replace the final stage of texture work and localised sculpted detail, which, as identified in Section 9, still necessitate manual intervention by an artist. The distinction between what a procedural, literature-grounded system can achieve and what must still be accomplished manually represents the most significant outcome of this project.

References

Bournemouth University, National Centre for Computer Animation (NCCA). (n.d.). NCCA Coding Standard - Using AI Coding Assistants. https://nccastaff.bournemouth.ac.uk/jmacey/NCCACodingStandard/AI_Coding/

Campobasso, C. P., Di Vella, G., & Introna, F. (2001). Factors affecting decomposition and Diptera colonization. Forensic Science International, 120(1–2), 18–27.

Connor, M., Baigent, C., & Hansen, E. S. (2018). Testing the use of pigs as human proxies in decomposition studies. Journal of Forensic Sciences, 63(5), 1350–1355.

Griffiths, K., Krosch, M. N., & Wright, K. (2020). Variation in decomposition stages and carrion insect succession in a dry tropical climate and its effect on estimating postmortem interval. Forensic Sciences Research, 5(4), 327–335.

Jani, G., & Johnson, A. (2021). Virtual reality and its transformation in forensic education and research practices. Journal of Visual Communication in Medicine, 45(1), 18–25.

Lengyel, E. (2012). Mathematics for 3D Game Programming and Computer Graphics (3rd ed.). Course Technology.

Matuszewski, S., Hall, M. J., Moreau, G., Schoenly, K. G., Tarone, A. M., & Villet, M. H. (2020). Pigs vs people: the use of pigs as analogues for humans in forensic entomology and taphonomy research. International Journal of Legal Medicine, 134(2), 793–810.

Matuszewski, S., Konwerski, S., Frątczak, K., & Szafałowicz, M. (2014). Effect of body mass and clothing on decomposition of pig carcasses. International Journal of Legal Medicine, 128(6), 1039–1048.

Mayne, R., & Green, H. (2020). Virtual reality for teaching and learning in crime scene investigation. Science & Justice, 60(5), 466–472.

Megyesi, M. S., Nawrocki, S. P., & Haskell, N. H. (2005). Using accumulated degree-days to estimate the postmortem interval from decomposed human remains. Journal of Forensic Sciences, 50(3), 618–626.

Mickleburgh, H. L. (2018). Actualistic experimental taphonomy of inhumation burial. In P. M. Barone & W. J. M. Groen (Eds.), Multidisciplinary Approaches to Forensic Archaeology (pp. 105–114). Springer.

Moffatt, C., Simmons, T., & Lynch-Aird, J. (2016). An improved equation for TBS and ADD: Establishing a reliable postmortem interval framework for casework and experimental studies. Journal of Forensic Sciences, 61(S1), S201–S207.

Owings, C. G., McKee-Zech, H. S., Patrick, E. A., & Steadman, D. W. (2025). A blow fly (Diptera: Calliphoridae) pre-colonization interval dataset for improving forensic entomology estimations. Journal of Forensic Sciences, 70(6), 2393–2402.

Owings, C. G., McKee-Zech, H. S., Schwing, S. T., Bugajski, K. N., Davis, M. C., & Steadman, D. W. (2022). Not by the book: Observations of delayed oviposition and re-colonization of human remains by blow flies. Insects, 13(10), 879.

Payne, J. A. (1965). A summer carrion study of the baby pig, Sus scrofa Linnaeus. Ecology, 46(5), 592–602.

Smith, D. H., Ehrett, C., Weisensee, K., & Tica, C. (2023). Commentary on: Megyesi et al. (2005) and Moffatt et al. (2016). Journal of Forensic Sciences, 68(1), 355–358.

Sutherland, A., Myburgh, J., Steyn, M., & Becker, P. J. (2013). The effect of body size on the rate of decomposition in a temperate region of South Africa. Forensic Science International, 231(1–3), 257–262.

The Gnomon Workshop. (2025). Procedural workflows for games using Houdini [Online course]. https://www.thegnomonworkshop.com/workshops/procedural-workflows-for-games-using-houdini

Trandzhiev, M., Koundouras, T., Milev, M., Laleva, L., Mitev, A., Stoykov, V., Dimitrov, N., Maslarski, I., Nakov, V., & Spiriev, T. (2024). The evaluation of virtual reality neuroanatomical training utilizing photorealistic 3D models in limited body donation program settings. Cureus, 16(3), e55377.

Tynan, P. (2023). Unveiling decomposition dynamics: Leveraging 3D models for advanced forensic analysis. International Journal of Legal Medicine, 138, 895–897. https://doi.org/10.1007/s00414-023-03142-7

Vass, A. A., Bass, W. M., Wolt, J. D., Foss, J. E., & Ammons, J. T. (1992). Time since death determinations of human cadavers using soil solution. Journal of Forensic Sciences, 37(5), 1236–1253.

Vass, A. A., Barshick, S. A., Sega, G., Caton, J., Skeen, J. T., Love, J. C., et al. (2002). Decomposition chemistry of human remains: A new methodology for determining the postmortem interval. Journal of Forensic Sciences, 47(3), 542–553.

Wescott, D. J., Steadman, D. W., Miller, N., Sauerwein, K., Clemmons, C. M. J., Gleiber, D. S., McDaneld, C., Meckel, L., & Bytheway, J. A. (2018). Validation of the total body score/accumulated degree-day model at three human decomposition facilities. Forensic Anthropology, 1(3), 143–149.

Appendix: Acknowledgement of Generative AI Use

I have not attributed any content generated by artificial intelligence as my own. I recognise the role played by Claude (Anthropic) in producing material which has been included in this essay in altered form, and in providing background research, structuring and drafting assistance while producing this assessment.

Drafting and restructuring assistance was used across this report: the author supplied the underlying factual record -the development history, the node-level architecture, the measured figures, the identified faults, and the forensic literature already reviewed in the accompanying thesis -and the AI assistance concerned reorganisation, connective prose, and expression of that material into the report structure, rather than the generation of new technical claims. All measurements taken from the Houdini asset, all comparisons against the forensic taphonomy literature, and all design decisions in the procedural graph are the author's own work, carried forward from the development record and thesis into this report.

Per-component detail -including the AI systems and versions used, the prompts issued, the outputs returned, the modifications made, and the verification carried out -is provided in the AI use declaration submitted with the project files, prepared in accordance with the NCCA Coding Standard on the use of AI coding assistants (Bournemouth University, NCCA, n.d.; see References). The associated chat logs are submitted alongside it.

Full citation for that standard: Bournemouth University, National Centre for Computer Animation (NCCA). (n.d.).NCCACodingStandard:UsingAICodingAssistants.
https://nccastaff.bournemouth.ac.uk/jmacey/NCCACodingStandard/AI_Coding/